Pulmonary vein stenosis and the pathophysiology of "upstream" pulmonary veins

Hideyuki Kato, MD,[a] Yaqin Yana Fu, MD, MS,[a] Jiaquan Zhu, MD, PhD,[a] Lixing Wang, MD, PhD,[a] Shabana Aafaqi, MSc,[a] Otto Rahkonen, MD,[b] Cameron Slorach, RDCS,[b] Alexandra Traister, PhD,[a] Chung Ho Leung, BSc,[a] David Chiasson, MD,[c] Luc Mertens, MD, PhD,[b] Lee Benson, MD,[b] Richard D. Weisel, MD, BA,[d] Boris Hinz, PhD,[e] Jason T. Maynes, MD, PhD,[f] John G. Coles, MD,[a] and Christopher A. Caldarone, MD[a]

Background: Surgical and catheter-based interventions on pulmonary veins are associated with pulmonary vein stenosis (PVS), which can progress diffusely through the "upstream" pulmonary veins. The mechanism has been rarely studied. We used a porcine model of PVS to assess disease progression with emphasis on the potential role of endothelial-mesenchymal transition (EndMT).

Methods: Neonatal piglets underwent bilateral pulmonary vein banding (banded, n = 6) or sham operations (sham, n = 6). Additional piglets underwent identical banding and stent implantation in a single-banded pulmonary vein 3 weeks postbanding (stented, n = 6). At 7 weeks postbanding, hemodynamics and upstream PV pathology were assessed.

Results: Banded piglets developed pulmonary hypertension. The upstream pulmonary veins exhibited intimal thickening associated with features of EndMT, including increased transforming growth factor (TGF)-β1 and Smad expression, loss of endothelial and gain of mesenchymal marker expression, and coexpression of endothelial and mesenchymal markers in banded pulmonary vein intimal cells. These immunopathologic changes and a prominent myofibroblast phenotype in the remodeled pulmonary veins were consistently identified in specimens from patients with PVS, in vitro TGF-β1-stimulated cells isolated from piglet and human pulmonary veins, and human umbilical vein endothelial cells. After stent implantation, decompression of a pulmonary vein was associated with reappearance of endothelial marker expression, suggesting the potential for plasticity in the observed pathologic changes, followed by rapid in-stent restenosis.

Conclusions: Neonatal pulmonary vein banding in piglets recapitulates critical aspects of clinical PVS and highlights a pathologic profile consistent with EndMT, supporting the rationale for evaluating therapeutic strategies designed to exploit reversibility of upstream pulmonary vein pathology. (J Thorac Cardiovasc Surg 2014;148:245-53)

Pulmonary vein stenosis (PVS) can occur as either a primary congenital or an acquired disease after repair of total anomalous pulmonary venous drainage (TAPVD).[1-3] A unique characteristic of PVS is the potential for progressive and diffuse stenosis throughout the pulmonary venous system. Although commonly manifest as a local stenosis at the pulmonary vein–left atrial junction, the most malignant form of the disease is characterized by diffuse involvement of the "upstream" pulmonary veins extending into the lung parenchyma. With the diffuse upstream lesion, PVS leads to relentless pulmonary hypertension, right heart failure, and death. Despite scattered recent reports of catheter-based interventions and surgical procedures,[4,5] the overall prognosis is poor.[6-9] Remarkably, the cellular mechanisms and pathophysiology that cause upstream PVS remain incompletely explored.

To investigate the cellular mechanisms associated with PVS, we used a neonatal piglet model previously established by LaBourene and colleagues,[10] with the objective of examining the histopathology of upstream PVS to characterize the diffuse fibrogenic response in the pulmonary veins. Our results suggest that endothelial-mesenchymal transition (EndMT) contributes to the propagation of the disease into the upstream pulmonary veins. By using cellular markers of EndMT, we characterized the disease process in the piglet model and found correlative data derived from pulmonary vein cell culture systems and

From the Division of Cardiovascular Surgery,[a] Hospital for Sick Children, Labatt Family Heart Center and University of Toronto; the Divisions of Cardiology[b] and Anaesthesia and Pain Medicine and Molecular Structure and Function,[f] Hospital for Sick Children; the Division of Pathology and Paediatric Laboratory Medicine,[c] Laboratory of Tissue Repair and Regeneration, University of Toronto, Hospital for Sick Children; the Division of Cardiac Surgery,[d] Toronto General Hospital; and the Laboratory of Tissue Repair and Regeneration,[e] Matrix Dynamics Group, Faculty of Dentistry, University of Toronto, Toronto, Ontario, Canada.

This study was supported by the Saving Tiny Hearts Society.

Disclosures: Authors have nothing to disclose with regard to commercial support.

Received for publication June 6, 2013; revisions received Aug 10, 2013; accepted for publication Aug 16, 2013; available ahead of print Sept 30, 2013.

Address for reprints: Christopher A. Caldarone, MD, Division of Cardiac Surgery, University of Toronto, Watson Family Chair in Cardiovascular Science–Labatt Family Heart Center Hospital for Sick Children, 555 University Ave, Toronto, ON, Canada, M5G 1X8 (E-mail: christopher.caldarone@sickkids.ca).

0022-5223/$36.00

http://dx.doi.org/10.1016/j.jtcvs.2013.08.046

Abbreviations and Acronyms

EndMT = endothelial-mesenchymal transition
FSP = fibroblastic-specific protein
GAPDH = glyceraldehyde-3-phosphate dehydrogenase
HCI = high-content imaging
HE = hematoxylin and eosin
HUVEC = human umbilical vein endothelial cell
PVS = pulmonary vein stenosis
SMA = smooth muscle actin
TAPVD = total anomalous pulmonary venous drainage
TGF = transforming growth factor
VE = vascular endothelial
vWF = von Willebrand factor VIII

autopsy-derived human specimens. Consistent with prior reports,[9] pulmonary vein stenting to relieve obstruction was associated with rapid in-stent restenosis. However, we observed evidence of regression of the pathologic process in the upstream pulmonary veins after stenting, suggesting an element of reversibility at the cellular level and highlighting new avenues of investigation.

METHODS

Research Ethics Board Approval

The Animal Care Committee at the Hospital for Sick Children approved the animal studies in accordance with the Terms of Reference following the Canadian Council on Animal Care Guidelines and federal/provincial legislations. Human samples were acquired with approval of the Research Ethics Board protocols under the auspices of the Heart Centre Biobank Registry (No. 1000011232 and No. 0020010432).

Piglet Pulmonary Vein Stenosis Model

One-week-old Yorkshire piglets (3.9 ± 0.8 kg) underwent staged bilateral pulmonary vein banding (banded, n = 6) or sham operations (sham, n = 6). After anesthesia and intubation, piglets underwent staged operations, as previously described.[10] Banding of left pulmonary veins and the common lower pulmonary vein was performed via a left fifth intercostal space thoracotomy, followed by banding of right pulmonary veins 1 week later, using one-eighth inch–wide cotton umbilical tapes with a length equivalent to 1.3 times the pulmonary vein circumference. Sham–operated on piglets underwent identical banding procedures, but the band was not left in place.

Echocardiography was performed under anesthesia before banding/sham operation and at 3 and 6 weeks postprocedure. At 7 weeks after bilateral banding/sham procedures, the piglets were anesthetized and instrumented to monitor hemodynamic parameters using 5F thermodilution catheters (Teleflex, Limerick, Pa). Cardiac output was determined by injection of 23 ± 1°C saline (5 mL) into the main pulmonary artery and calculated with a cardiac output computer (model 9520A; Edwards Lifesciences, Irvine, Calif). Lung biopsy specimens were taken from each left distal middle lobe. The heart and lungs were quickly removed en bloc and dissected on a bed of ice. The upstream pulmonary veins were obtained, excluding pulmonary veins within the first 10 mm from banded sites, and divided into sections for the primary cell culture, fixed in 10% formalin, or frozen. Hematoxylin and eosin (HE) staining was used to show the intimal thickness and pulmonary vein morphology. Intimal thickness was assessed by measurement of the ratio of intimal to intimal + medial layer thickness at 8 radial points in each pulmonary vein.

Stent Implantation

Another 6 piglets were allotted for stent treatment (stented, n = 6). Three weeks after identical bilateral pulmonary vein banding with the banded group, the stented group underwent placement of bare-metal stents (Driver; Medtronic Inc, Minneapolis, Minn) into the right middle pulmonary vein via femoral vein catheterization with 8F sheaths under fluoroscopic and intracardiac echocardiographic guidance (8F AcuNav catheter; Biosense Webster, Diamond Bar, Calif). After atrial septum puncture with a pediatric transseptal needle (COOK, Bloomington, Ind), using a 6F RunWay WRP guide catheter (Boston Scientific Corp, Natick, Mass), bare-metal stents (3.5- or 4.0-mm in diameter) were deployed into the banding site of the right middle pulmonary vein. Acetylsalicylic acid, 10 mg/kg per day (Tanta Pharmaceuticals Inc, Whitby, Ontario, Canada), and clopidogrel, 2.5 mg/kg per day (Teva Canada, Ontario, Canada), were given orally until the end point of the study. At 7 weeks postbanding, invasive hemodynamics were measured and tissues were excised, as previously described. The stented portions of the pulmonary veins were excised and cross-sectioned at 3 points within the stent (proximal, middle, and distal) cut by an Isomet slow-speed saw (Buehler, Lake Bluff, Ill) and tungsten carbide knife. The percentage of in-stent restenosis was quantified using Image J software (National Institutes of Health, Bethesda, MD), according to the following formula: 100 × (ICM [minus] LA)/ICM, where ICM is the inner area of the internal circumference of the media and LA is the inner area of internal circumference of the intima.[11-13]

Human Tissue

Pulmonary vein specimens were obtained from 3 patients with PVS. One patient had recurrent PVS after TAPVD repair (2 days of age), followed by reoperation for progressive PVS (3 months of age) and subsequent death. Autopsy specimens were stained for immunofluorescence, as described later (Figure 1, *C-G*). A second patient, with a diagnosis of tetralogy of Fallot and PVS, underwent intracardiac repair and pulmonary vein stent implantation at the age of 17 months. However, subsequent in-stent restenosis and severe pulmonary hypertension resulted in death at the age of 20 months. At autopsy, Movat pentachrome staining was performed to assess the PV morphology in 1 patient (Figure 1, *A*). A third patient, diagnosed with hypoplastic left heart syndrome, had recurrent refractory PVS after heart transplant at the age of 5 months and died at the age of 9 months. Elastic Masson trichrome staining of the pulmonary veins was used at autopsy (Figure 1, *B*).

Control human pulmonary vein tissues were obtained from a heart transplant donor who was 2 months old and did not have pulmonary vascular disease; they were analyzed using the same immunofluorescence protocols (Figure 1, *H-L*) and cultured for high-content imaging (HCI) analysis.

Right Ventricle Cellular Size and Myocardial Fibrosis

Transmural blocks of the right ventricular myocardium were fixed in 10% formalin, divided into sections, and stained with HE and Masson trichrome stains.[14] Randomly selected high-power fields (400×, 60 fields per piglet) from right ventricular free walls were examined for analysis of cellular size and cardiac fibrosis. The diameter of cells was determined by measuring the distance across the cell at its narrowest plane, including the nucleus (Image J software). The area of myocardial collagen content for each field was quantified (Photoshop CS4; Adobe Systems, San Jose, Calif) as a percentage of the entire slide and averaged.

Immunofluorescence

Paraffin-embedded tissue slides were deparaffinized in xylene and rehydrated in ethanol. Antigens were remasked with sodium citrate buffer

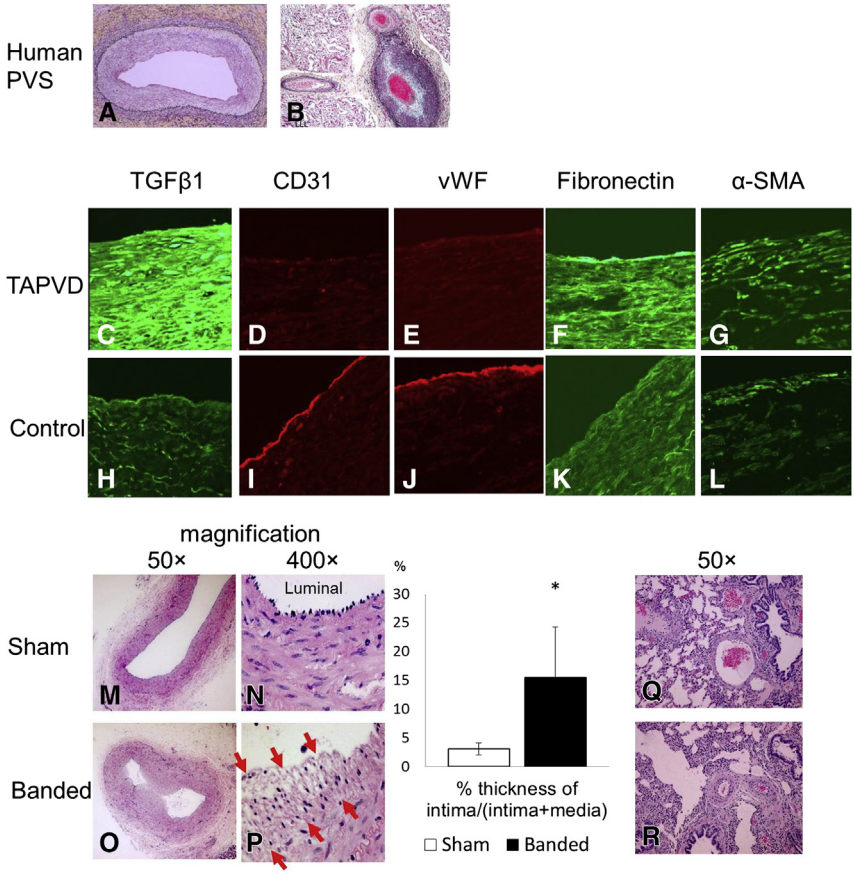

FIGURE 1. Histology and immunofluorescence staining in human and piglet pulmonary veins. A, Human pulmonary vein histology from a patient with pulmonary vein stenosis (*PVS*); Movat pentachrome staining showed fibromuscular hyperplasia. B, Human PVS lung tissue; elastic trichrome staining demonstrated marked pulmonary vein intimal hyperplasia (arterialization) with luminal narrowing. C-G, Pulmonary veins from a total anomalous pulmonary venous drainage (*TAPVD*) patient with PVS (400× magnification) compared with the control histology. H-L, Control pulmonary veins from a heart transplant donor without PVS; endothelial markers (CD31 and von Willebrand factor [*vWF*] in D and E) were decreased, and expression of transforming growth factor (*TGF*)-β1 (C) and mesenchymal markers (fibronectin and α-smooth muscle actin [*SMA*] in F and G) were increased in the TAPVD patient, consistent with the piglet study. M-P, Hematoxylin and eosin staining of upstream pulmonary veins in the piglet model. M and N, Sham group. O and P, Banded group. Banded PVs had increased intimal thickness (*red arrows* in P). Intimal thickness as percentage of intimal + medial layer thickness was greater in banded pulmonary veins. $*P < .05$. Q and R, Representative microvascular changes in the lung. Q, Lung tissue in the sham group had thin-walled pulmonary veins. R, Lung tissue in the banded group had intimal hyperplasia in pulmonary veins.

(Dako, Glostrup, Denmark), then immersed in blocking buffer for 40 minutes and incubated with primary antibodies CD31 (1:100; Abcam, Cambridge, UK), fibronectin (1:200; BD Transduction Laboratories, Franklin Lakes, NJ), vascular endothelial cadherin (VE-cadherin, 1:100; Thermo Fisher Scientific, Waltham, Mass), α-smooth muscle actin (α-SMA, 1:100; Santa Cruz Biotechnology, Santa Cruz, Calif), fibroblastic-specific protein 1 (FSP-1)/S100A4 (1:100; Millipore, Billerica, Mass), von Willebrand factor VIII (vWF, 1:100; Dako), and transforming growth factor (TGF)-β1 (1:100; Abcam) for 2 hours at room temperature, followed by the secondary anti-rabbit antibody (1:1000) and anti-mouse fluorescein isothiocyanate (1:100) for 1 hour at room temperature. Slides were visualized using a Quorum WaveFX-X1 Spinning Disc Confocal System (Quorum Technologies, Guelph, Ontario, Canada) and Volocity software (PerkinElmer Inc, Waltham, Mass).

Protein Extraction and Western Blot Analysis

Upstream PV samples from piglets were homogenized in lysis buffer and centrifuged for 20 minutes at 13,400*g* at 4°C, and the supernatants were collected. Protein extracts were quantified with a Bradford protein assay (Bio-Rad, Hercules, Calif).

Samples were separated on 10% polyacrylamide gels, transferred to nitrocellulose membranes, and blocked with 5% skimmed milk for 1 hour. The membranes were probed with CD31 (1:1000), VE-cadherin (1:1000), α-SMA (1:1000), TGF-β1 (1:1000), Smad4 (1:500; Abcam), and glyceraldehyde-3-phosphate dehydrogenase (GAPDH; 1:6000; Sigma-Aldrich, St Louis, Mo). Blots were then incubated with goat anti-mouse IgG horseradish peroxidase (1:10,000) and goat anti-rabbit IgG horseradish peroxidase (1:5000) secondary antibodies. Membranes were developed with electrochemiluminescence substrate (Santa Cruz Biotechnology). Densitometry was analyzed using Quantity One and Image Lab analysis software (Bio Rad Laboratories, Hercules, Calif). GAPDH was used to verify all protein loads and normalize data.

Isolation and Cell Culture

Pulmonary vein samples from piglets and humans were minced and washed with phosphate-buffered saline. Cell isolation was performed

with 5% trypsin and 1 mg/mL type II collagenase in 20% glucose phosphate-buffered saline at 37°C (pH 7.4). After isolation, the cells were cultured in Iscove modified Dulbecco medium (Life Technologies, Carlsbad, Calif) with antibiotics and incubated in 5% CO_2 at 37°C. Human umbilical vein endothelial cells (HUVECs) were purchased from ATCC (Manassas, Va) and cultured.

Cultured human PV cells from a heart transplant donor, banded piglet PV cells, and HUVECs were treated with 5 ng/mL recombinant human TGF-β1 (R&D Systems Inc, Minneapolis, Minn) for 48 hours to mimic the EndMT process.[15] Cells that were not treated with TGF-β1 served as controls. Then, 96- or 384-well plates were used to grow, stain, image, and analyze cells in a semiautomated manner using HCI to increase reliability and statistical significance. Immunofluorescence was performed using the fibronectin (1:100) and α-SMA (1:100) antibodies. Nuclei were stained with Hoechst (1×). Samples were imaged in a Cellomics VTI automated high-content imager and analyzed using a combination of Image J and custom-written software. For all 3 cell types, more than 400 cells per condition were tested, in triplicate.

Statistical Analysis

Continuous variables were expressed as mean ± SEM. The unpaired *t* test was used for comparisons in echocardiographic data, Western blot analysis data, and intimal thickness data between the banded and sham groups. Multiple group comparisons between sham, banded, and stented groups were compared by 1-way analysis of variance, followed by the Tukey post hoc test. HCI statistics were generated using custom scripts written for the R software package (Vienna, Austria) and represented as Winsorized means (5% tails), and *P* values were calculated by Mann-Whitney test.

CHD

RESULTS

Human PVS Induces a Decrease in Endothelial and Gain of Mesenchymal Markers in the Hyperplastic Intima

Histology staining in PV tissues from patients with progressive PVS demonstrated fibromuscular hyperplasia in the intima of the pulmonary veins (Figure 1, *A*) and arterialization of a pulmonary vein with marked luminal narrowing (Figure 1, *B*). In the patient with obstructed TAPVD, immunofluorescence showed that the pulmonary veins had greater expression of fibronectin and α-SMA, had diminished expression of CD31 and vWF, and exhibited stronger TGF-β1 expression compared with control human pulmonary veins (Figure 1, *C-L*). The loss of endothelial markers and gain of mesenchymal markers indicated a possible phenotypic conversion of the endothelium into reparative myofibroblasts.

Banding of the Pulmonary Veins Reproduces Functional Consequences of Human PVS in a Porcine Model

Six weeks postbanding, echocardiography demonstrated that the pulmonary vein gradient increased progressively to 11.50 ± 4.76 mm Hg in the banded animals (vs 3.40 ± 3.36 mm Hg in the sham group; $P < .01$).

Consistent with PVS in human patients, banding of porcine pulmonary veins induced changes in hemodynamics. At 7 weeks postprocedure, banded piglets had equivalent central venous pressure (4.83 ± 4.08 vs 1.83 ± 1.47 mm Hg), higher pulmonary capillary wedge pressure (11.33 ± 3.07 vs 5.33 ± 2.14 mm Hg; $P = .01$), systolic right ventricular pressure (38.8 ± 8.77 vs 19.50 ± 2.43 mm Hg; $P < .01$), and mean pulmonary arterial pressure (34.3 ± 8.89 vs 12.0 ± 2.37 mm Hg; $P < .01$) compared with sham animals. The ratio of mean pulmonary arterial pressure to mean systemic blood pressure was higher in banded piglets than in sham piglets (0.65 ± 0.18 vs 0.23 ± 0.02 mm Hg; $P < .01$). Cardiac output was not different between groups (0.14 ± 0.02 vs 0.15 ± 0.02 L/min per kg; $P = .25$). Banded piglets had higher pulmonary vascular resistance (7.54 ± 2.91 vs 1.44 ± 0.24 mm Hg/L per minute; $P < .01$) and lower pulmonary vascular compliance (1.45 ± 1.11 vs 7.20 ± 1.57 mL/mm Hg; $P < .01$).

Banded piglets had more right ventricle (RV) hypertrophy compared with sham animals, as assessed by the ratio of right ventricular weight to left ventricular plus ventricular septal weight (RV/LV + septum, 0.65 ± 0.10 vs 0.35 ± 0.02; $P = .01$). Histologic and morphologic analysis demonstrated RV hypertrophy manifested with a greater average diameter of RV myocytes in the banded group (16.67 ± 1.12 vs 13.95 ± 1.80 μm; $P = .02$) and a higher percentage of collagen deposition in the RV of the banded group compared with the sham group (7.96% ± 2.66% vs 2.88% ± 1.02%; $P = .01$).

Stent implantation in a single pulmonary vein at 3 weeks after banding did not improve overall hemodynamics. There were no significant differences in any hemodynamic parameters when comparing stented with nonstented banded piglets 7 weeks postbanding.

Banding of Porcine Pulmonary Veins Mimics the Intimal Morphologic Changes Observed in Human PVS

Morphologic changes in upstream pulmonary veins from the banded piglets were analyzed. These veins had greater intimal thickness compared with sham piglets (15.48% ± 8.76% vs 3.07% ± 1.04%; $P < .01$) (Figure 1, *M-P*). Small pulmonary veins in the distal lung parenchyma had greater intimal hyperplasia and luminal stenosis compared with sham piglets (Figure 1, *Q* and *R*). Next, we assessed fibroproliferative changes in upstream banded pulmonary veins by immunofluorescence and Western blotting. Compared with sham piglets, the upstream pulmonary veins in banded piglets had greater expression of the mesenchymal markers, fibronectin and FSP-1, and myofibroblast marker, α-SMA (Figure 2, *A-F*). Western blot analysis confirmed greater expression of α-SMA in upstream banded pulmonary veins compared with sham piglets (α-SMA/GAPDH, 1.03 ± 0.26 vs 1.38 ± 0.26; $P = .028$; Figure 2).

To test whether fibroproliferative changes affected distribution and expression of endothelial markers, we immunostained for CD31, vWF, and VE-cadherin. Expression of all endothelial markers decreased in upstream banded pulmonary veins (Figure 2, *G-L*), similar to the changes seen in human

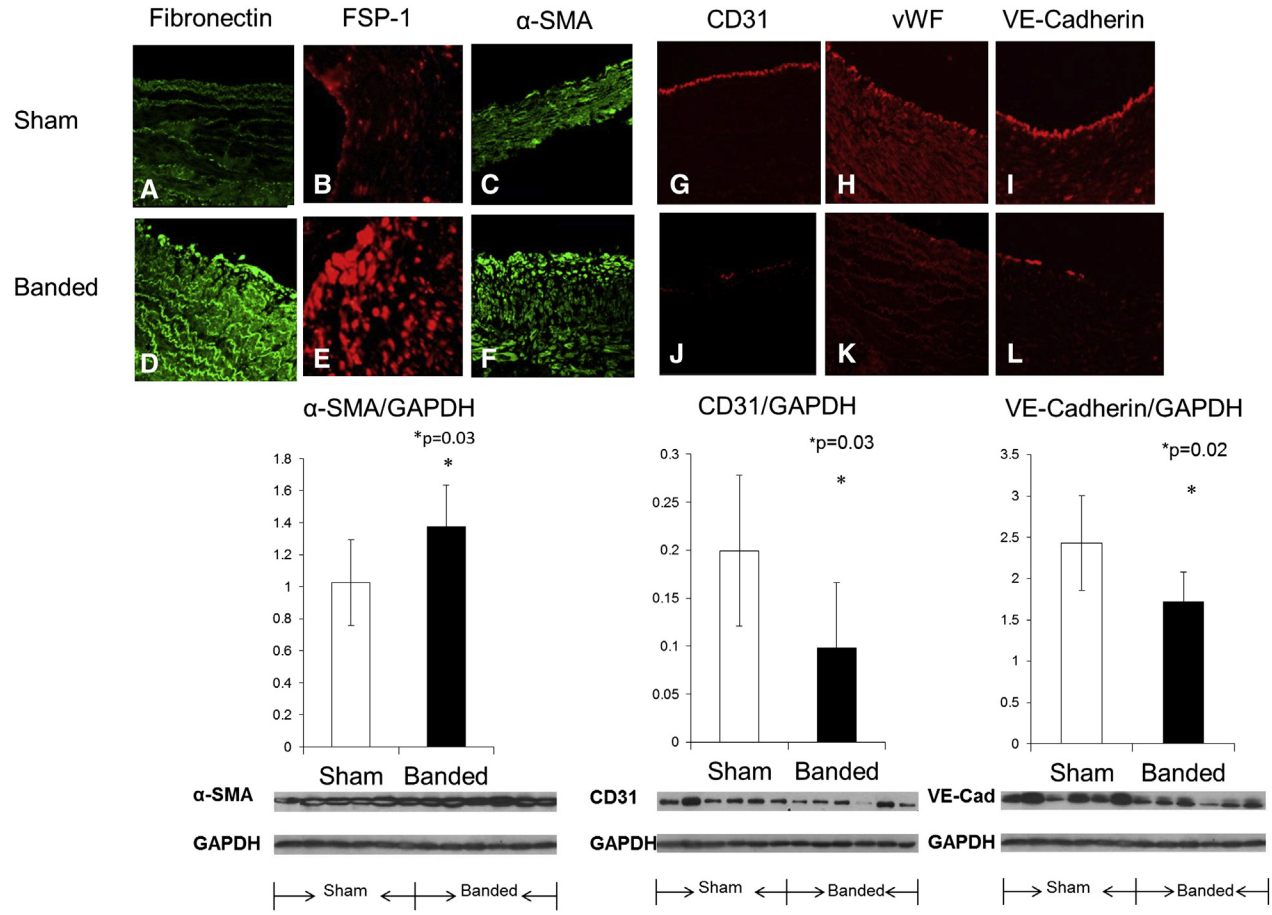

FIGURE 2. Representative gain of mesenchymal and decrease of endothelial markers in immunofluorescent staining of upstream pulmonary veins of the piglet pulmonary vein stenosis (*PVS*) model. A-C, G, and I, Upstream pulmonary veins in the sham group. D-F and J-L, Upstream pulmonary veins in the banded group. Banded pulmonary veins exhibited greater expression of mesenchymal markers (fibronectin, fibroblast-specific protein [*FSP*]-*1*, and α-smooth muscle actin [*SMA*] in A-F; 400× magnification) and less expression of endothelial markers (CD31, von Willebrand factor [*vWF*], and vascular endothelial [*VE*]-cadherin in G-L; 400× magnification) compared with sham pulmonary veins. The banded upstream pulmonary vein demonstrated increased expression of α-SMA and decreased expression of CD31 and VE-cadherin in Western blot analysis. *GAPDH*, Glyceraldehyde-3-phosphate dehydrogenase. $*P < .05$.

PVS samples (Figure 1). Western blotting confirmed lower expression of the endothelial markers, CD31 and VE-cadherin, in banded piglet pulmonary veins (CD31/GAPDH, 0.20 ± 0.08 vs 0.10 ± 0.07 [$P = .031$]; and VE-cadherin/GAPDH, 2.42 ± 0.58 vs 1.72 ± 0.36 [$P = .017$]) (Figure 2). Double immunostaining of CD31 and α-SMA was performed to investigate the pathologic process associated with transition of individual cells with coexpression of endothelial and mesenchymal markers. Imaging revealed intermittent intimal cells coexpressing endothelial and mesenchymal markers in banded pulmonary veins (transitional cell phenotype) (Figure 3, *G*). Coexpression of these markers was never observed in pulmonary veins of sham animals.

Intimal Hyperplasia After Pulmonary Vein Banding Is Associated With Profibrotic Signaling Events

One of the major drivers of EndMT is TGF-β-mediated signaling events that involve phosphorylation and subsequent nuclear translocation of Smad.[16,17] Expression of TGF-β1 in the pulmonary veins was greater in banded compared with sham piglets, consistent with the presence of EndMT (Figure 3, *H* and *I*). Quantitatively, Western blot analysis demonstrated increased expression of TGF-β1 and Smad 4 in banded upstream PVs compared with unbanded PVs (TGF-β1/GAPDH, 1.15 ± 0.32 vs 1.73 ± 0.34 [$P = .01$]; Smad 4/GAPDH, 0.50 ± 0.15 vs 0.76 ± 0.24 [$P = .05$]; Figure 3).

Stent Implantation Partially Reverses the Changes Induced by Experimental PVS

In-stent restenosis reduced the luminal diameter within the stent by $43\% \pm 28\%$ at 4 weeks after stent implantation in the porcine model (Figure 4, *K*). At 7 weeks after pulmonary vein banding (4 weeks after stent implantation), upstream pulmonary veins in the stented piglets demonstrated greater expression of TGF-β1 in comparison to

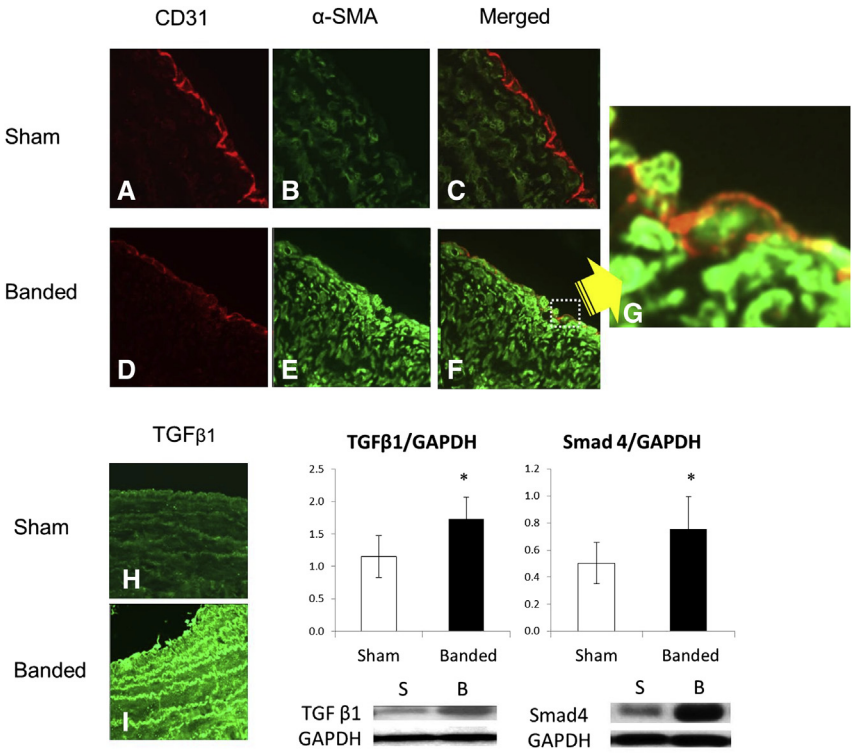

FIGURE 3. Coexpression of endothelial and mesenchymal markers confirming the presence of the endothelial-mesenchymal transition (*EndMT*) transitional cell phenotype. A-C, H, and I, Upstream pulmonary veins in the sham group. D-G, J, and K, Upstream pulmonary veins in the banded group. A-F, Immunofluorescence showed decreased endothelial and increased mesenchymal markers in banded pulmonary veins. G, In the banded group, intimal cells expressed an endothelial marker (CD31 in *red*) in the outer membrane and a mesenchymal marker (α-smooth muscle actin [*SMA*] in *green*) in the intracellular space, consistent with an EndMT transitional cell (600× magnification). H and I, Expression of transforming growth factor (*TGF*)-β1. Banded pulmonary veins demonstrated greater expression of TGF-β1 compared with sham pulmonary veins (400× magnification). Western blot analysis supported increased expression of TGF-β1 and Smad 4 in banded upstream pulmonary veins ($P = .01$ and $P = .049$, respectively). *Asterisks* refer to statistically significant comparisons. *GAPDH*, Glyceraldehyde-3-phosphate dehydrogenase; *S*, sham; *B*, banded.

sham animals but less expression than banded animals (by subjective evaluation of immunofluorescence images). These findings suggested partial down-regulation of TGF-β expression and partial reappearance of CD31 and vWF (endothelial marker) expression with enhanced and localized fibronectin and α-SMA (mesenchymal and myofibroblast markers) expression in the intima (Figure 4, *A-L*), consistent with partial reversal of the immunohistochemical features of EndMT.

Three Types of Cultured Cells Are Prone to Experimentally Induced EndMT

All 3 cultured cell types (banded piglet PV cells, human control PV cells, and HUVECs) demonstrated increased expression of the myofibroblast markers, fibronectin and α-SMA, after TGF-β1 exposure (integrated fluorescence intensity, fibronectin: piglet cells, 1008 ± 89 vs 1044 ± 120 [$P < .05$]; human cells, 3918 ± 111 vs 4836 ± 123 [$P < .05$]; HUVECs, 1418 ± 102 vs 2160 ± 176 [$P < .01$]; α-SMA: piglet cells, 3679 ± 167 vs 5935 ± 400 [$P < .01$]; HUVECs, 1882 ± 160 vs 2072 ± 189 [$P < .05$]; Figure 5). The increase in the myofibroblast markers suggests that stimulation with TGF-β1 recapitulates the pathologic process observed in the in vivo animal model.

DISCUSSION

We previously investigated a piglet model of progressive PVS, which revealed increased pulmonary vascular resistance and degradation of the internal elastic lamina of the pulmonary veins.[10] The precise molecular pathways leading to the pulmonary venous fibrogenic response, however, remain unknown. The piglet model described herein recapitulates the critical aspects of clinical PVS, including myocardial alterations, hemodynamic sequelae, and histopathologic features, in the affected pulmonary veins. Examination of the cellular response in upstream pulmonary veins reveals a decrease of endothelial markers and a gain of mesenchymal markers, implicating a potential role for EndMT in the pathologic process. EndMT has also been observed to participate in several other fibrogenic diseases in which vascular remodeling is a critical

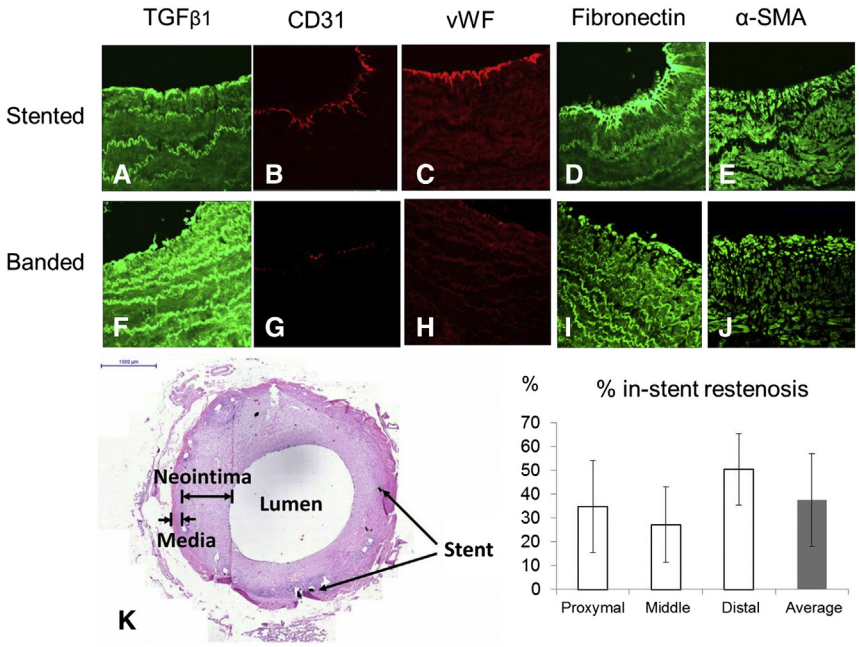

FIGURE 4. Representative immunofluorescent staining and hematoxylin and eosin (*HE*) staining of stented piglet pulmonary veins. A-E, Upstream pulmonary veins in the stented group. F-J, Upstream pulmonary veins in the banded group. Upstream pulmonary veins from stented piglets demonstrated moderately increased transforming growth factor (*TGF*)-β1 expression, regained endothelial markers (B and C), and strong expression of mesenchymal markers (D and E). K, Representative HE staining of pulmonary veins with a stent from a stented piglet demonstrated in-stent restenosis. *Arrow* indicates stent fragments inside the pulmonary venous wall (50× magnification). A graph below showed the percentage of in-stent restenosis 4 weeks poststenting in each stent area. Average area percentage of in-stent stenosis was 43.46% ± 27.85%. *vWF*, Von Willebrand factor; *SMA*, smooth muscle actin.

component of the pathologic process.[15,18-20] Other data suggesting a role for EndMT in the pathology include the finding of coexpression of endothelial and mesenchymal markers in the pulmonary vein intimal cells of banded piglets, albeit at low frequency. The presence of such coexpression has been cited as supportive evidence for the intermediate stage of EndMT.[18,21,22] In the current study, increased TGF-β and Smad 4 expression were also noted in the obstructed PVs from piglets. TGF-β is a well-known mediator of EndMT during cardiovascular development.[15,23-25] Smad is a downstream mediator in the TGF-β signaling pathways, with Smad 4 a common mediator interacting with receptor-regulated Smads, which, in turn, is associated with EndMT.[19,26-28]

Although local inflammation at the banding site may have a role in diffuse PVS, these data suggest that upstream

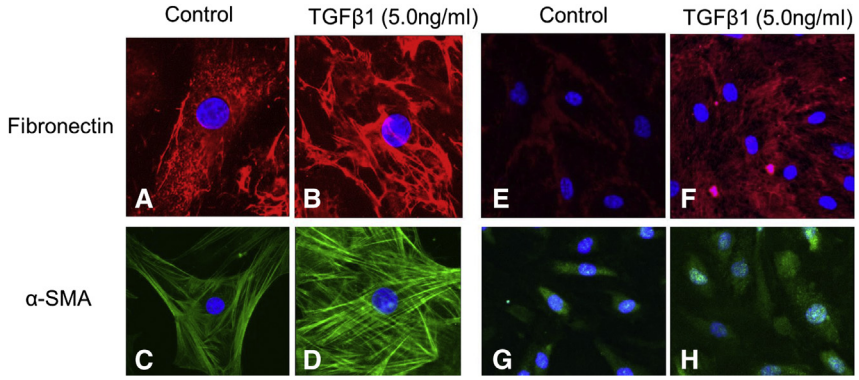

FIGURE 5. Induction of endothelial-mesenchymal transition (*EndMT*) in vitro high-content imaging of cultured piglet pulmonary vein cells and human umbilical vein endothelial cells (*HUVECs*). A and C, Control banded piglet pulmonary vein (*PV*) cells. B and D, Banded piglet PV cells treated with transforming growth factor (TGF)-β1 (5 ng/mL, 24 hours). E and G, Control HUVECs. F and H, HUVECs treated with TGF-β1 (5 ng/mL, 24 hours). The cells treated with TGF-β1 showed an increase in the myofibroblast markers, fibronectin and α-smooth muscle actin (*SMA*), capturing the EndMT transitional process ($P < .05$ vs control).

pulmonary vein endothelial injury is associated with elaboration of TGF-β, Smad signaling events, and proliferation of myofibroblasts in the pulmonary vein wall. Local inflammation from the banding material does, however, represent a limitation of our model. We have attempted to mitigate this limitation by examining the ''upstream'' pulmonary veins at locations that were 10 to 40 mm away from the banding site. We believe this distance is beyond the range of local inflammation. Although difficult to precisely identify, the geometric extent of the local inflammatory effect, the examined upstream areas, appeared on gross inspection to be free of obvious induration. Furthermore, our histologic examination was consistent with human samples in which there were no implanted foreign bodies to create PVS.

Although our data were consistent with a role for EndMT in the observed pulmonary venous pathology, other mechanisms alone or in combination with EndMT may account for the fibrogenic response in the upstream pulmonary veins. The increased number of myofibroblasts may be derived from proliferation of local or migrating resident mesenchymal cells[29,30] or may originate from circulating progenitor cells.[31,32] We propose that, irrespective of its putative origin, however, the myofibroblast is the culprit cell in the pathogenesis of PVS.

The use of high-content imaging in the present study demonstrates that TGF-β induces a myofibroblast phenotype in human and piglet pulmonary veins and in HUVECs. We propose that this cell-based assay, suitable for high-throughput screening, emulates a critical element in the genesis of PVS and could be used to evaluate libraries of compounds for their capacity to inhibit this process. This would advance the objective of developing therapeutic agents designed to target TGF-β1–mediated transformation and the disease-relevant molecular pathways leading to PVS.

Few studies have evaluated the effect of stent implantation in obstructed pulmonary veins, and these studies tend to focus on in-stent restenosis rather than the histopathology of the upstream pulmonary veins. Indeed, we noted significant in-stent restenosis within 4 weeks of stent placement, which is consistent with the limited efficacy of stents to treat pediatric PVS.[9] Furukawa and colleagues[13] evaluated the effectiveness of drug-eluting stents in pig pulmonary veins. However, in their study, the stents were deployed in unobstructed pulmonary veins. In contrast, our report is the first, to our knowledge, to evaluate the efficacy of stents in a model of progressive PVS. Future studies to test the efficacy of stents may be more informative if performed in the setting of an experimental model of PVS. The piglet model is a ''high-yield'' model because there is ample opportunity to study mechanisms of upstream PVS, in-stent restenosis, and right ventricular failure due to pressure overload (beyond the scope of the current article).

Despite the temporary reduction of obstruction, upstream pulmonary veins responded to stent implantation with some return of endothelial markers, suggesting the potential for plasticity in the observed pathophysiologic process. Reversal of EndMT is known to occur (ie, mesenchymal-endothelial transition).[33] Stenting appears to have initiated some reversal of the process, possibly because of temporary relief of local pulmonary venous hypertension. Rapid in-stent restenosis, however, likely limited the efficacy of the intervention. We need to study more time points after stent implantation to better characterize the alterations in pulmonary venous pathology associated with relief of obstruction. The origin of the cells expressing endothelial markers after stenting is unclear, and these cells could arise from mesenchymal-endothelial transition, circulating endothelial progenitor cells,[34,35] or enhanced reexpression from native endothelial cells. Although the mechanism is unclear, the potential for reversibility of the pathologic process warrants further investigation to develop novel adjuvant therapies designed to promote reversal of the process in concert with local surgical and stent-based decompression of pulmonary vein stenosis.

We thank Wei Hui from Heart Centre Echocardiography Laboratory for performing echocardiography and appreciate the contribution of participating surgeons, Drs Glen Van Arsdell, Osami Honjo, and Edward Hickey.

References

1. Humpl T, Reyes JT, Erickson S, Armano R, Holtby H, Adatia I. Sildenafil therapy for neonatal and childhood pulmonary hypertensive vascular disease. *Cardiol Young*. 2010;21:187-93.
2. Grosse-Wortmann L, Al-Otay A, Goo HW, Macgowan CK, Coles JG, Benson LN, et al. Anatomical and functional evaluation of pulmonary veins in children by magnetic resonance imaging. *J Am Coll Cardiol*. 2007;49:993-1002.
3. Karamlou T, Gurofsky R, Al Sukhni E, Coles JG, Williams WG, Caldarone CA, et al. Factors associated with mortality and reoperation in 377 children with total anomalous pulmonary venous connection. *Circulation*. 2007;115:1591-8.
4. Hickey EJ, Caldarone CA. Surgical management of post-repair pulmonary vein stenosis. *Semin Thorac Cardiovasc Surg Pediatr Card Surg Annu*. 2011;14:101-8.
5. Caldarone CA, Najm HK, Kadletz M, Smallhorn JF, Freedom RM, Williams WG, et al. Surgical management of total anomalous pulmonary venous drainage: impact of coexisting cardiac anomalies. *Ann Thorac Surg*. 1998;66:1521-6.
6. Caldarone CA, Najm HK, Kadletz M, Smallhorn JF, Freedom RM, Williams WG, et al. Relentless pulmonary vein stenosis after repair of total anomalous pulmonary venous drainage. *Ann Thorac Surg*. 1998;66:1514-20.
7. Viola N, Alghamdi AA, Perrin DG, Wilson GJ, Coles JG, Caldarone CA. Primary pulmonary vein stenosis: the impact of sutureless repair on survival. *J Thorac Cardiovasc Surg*. 2011;142:344-50.
8. Yun TJ, Coles JG, Konstantinov IE, Al-Radi OO, Wald RM, Guerra V, et al. Conventional and sutureless techniques for management of the pulmonary veins: evolution of indications from postrepair pulmonary vein stenosis to primary pulmonary vein anomalies. *J Thorac Cardiovasc Surg*. 2005;129:167-74.
9. Balasubramanian S, Marshall AC, Gauvreau K, Peng LF, Nugent AW, Lock JE, et al. Outcomes after stent implantation for the treatment of congenital and postoperative pulmonary vein stenosis in children. *Circ Cardiovasc Interv*. 2012;5:109-17.
10. LaBourene JI, Coles JG, Johnson DJ, Mehra A, Keeley FW, Rabinovitch M. Alterations in elastin and collagen related to the mechanism of progressive pulmonary venous obstruction in a piglet model: a hemodynamic, ultrastructural, and biochemical study. *Circ Res*. 1990;66:438-56.

11. Schwartz RS, Huber KC, Murphy JG, Edwards WD, Camrud AR, Vlietstra RE, et al. Restenosis and the proportional neointimal response to coronary artery injury: results in a porcine model. *J Am Coll Cardiol*. 1992;19:267-74.
12. Suzuki T, Kopia G, Hayashi SI, Bailey LR, Llanos G, Wilensky R, et al. Stent-based delivery of sirolimus reduces neointimal formation in a porcine coronary model. *Circulation*. 2001;104:1188-93.
13. Furukawa T, Kishiro M, Fukunaga H, Ohtsuki M, Takahashi K, Akimoto K, et al. Drug-eluting stents ameliorate pulmonary vein stenotic changes in pigs in vivo. *Pediatr Cardiol*. 2010;31:773-9.
14. Unverferth DV, Baker PB, Swift SE, Chaffee R, Fetters JK, Uretsky BF, et al. Extent of myocardial fibrosis and cellular hypertrophy in dilated cardiomyopathy. *Am J Cardiol*. 1986;57:816-20.
15. Arciniegas E, Frid MG, Douglas IS, Stenmark KR. Perspectives on endothelial-to-mesenchymal transition: potential contribution to vascular remodeling in chronic pulmonary hypertension. *Am J Physiol Lung Cell Mol Physiol*. 2007; 293:L1-8.
16. Masszi A, Kapus A. Smaddening complexity: the role of Smad3 in epithelial-myofibroblast transition. *Cells Tissues Organs*. 2011;193:41-52.
17. Chapman HA. Epithelial-mesenchymal interactions in pulmonary fibrosis. *Annu Rev Physiol*. 2011;73:413-35.
18. Zeisberg EM, Tarnavski O, Zeisberg M, Dorfman AL, McMullen JR, Gustafsson E, et al. Endothelial-to-mesenchymal transition contributes to cardiac fibrosis. *Nat Med*. 2007;13:952-61.
19. Kitao A, Sato Y, Sawada-Kitamura S, Harada K, Sasaki M, Morikawa H, et al. Endothelial to mesenchymal transition via transforming growth factor-beta1/Smad activation is associated with portal venous stenosis in idiopathic portal hypertension. *Am J Pathol*. 2009;175:616-26.
20. Hashimoto N, Phan SH, Imaizumi K, Matsuo M, Nakashima H, Kawabe T, et al. Endothelial-mesenchymal transition in bleomycin-induced pulmonary fibrosis. *Am J Respir Cell Mol Biol*. 2010;43:161-72.
21. Boonla C, Krieglstein K, Bovornpadungkitti S, Strutz F, Spittau B, Predanon C, et al. Fibrosis and evidence for epithelial-mesenchymal transition in the kidneys of patients with staghorn calculi. *BJU Int*. 2011;108:1336-45.
22. Vongwiwatana A, Tasanarong A, Rayner DC, Melk A, Halloran PF. Epithelial to mesenchymal transition during late deterioration of human kidney transplants: the role of tubular cells in fibrogenesis. *Am J Transplant*. 2005;5: 1367-74.
23. Zeisberg EM, Tarnavski O, Zeisberg M, Dorfman AL, McMullen JR, Gustafsson E, et al. Endothelial-to-mesenchymal transition contributes to cardiac fibrosis. *Nat Med*. 2007;13:952-61.
24. Ghosh AK, Nagpal V, Covington JW, Michaels MA, Vaughan DE. Molecular basis of cardiac endothelial-to-mesenchymal transition (EndMT): differential expression of microRNAs during EndMT. *Cell Signal*. 2012;24:1031-6.
25. Eisenberg LM, Markwald RR. Molecular regulation of atrioventricular valvuloseptal morphogenesis. *Circ Res*. 1995;77:1-6.
26. Mihira H, Suzuki HI, Akatsu Y, Yoshimatsu Y, Igarashi T, Miyazono K, et al. TGF-beta-induced mesenchymal transition of MS-1 endothelial cells requires Smad-dependent cooperative activation of Rho signals and MRTF-A. *J Biochem*. 2012;151:145-56.
27. van Meeteren LA, ten Dijke P. Regulation of endothelial cell plasticity by TGF-beta. *Cell Tissue Res*. 2012;347:177-86.
28. Medici D, Potenta S, Kalluri R. Transforming growth factor-beta2 promotes Snail-mediated endothelial-mesenchymal transition through convergence of Smad-dependent and Smad-independent signalling. *Biochem J*. 2011;437:515-20.
29. Yuen CY, Wong SL, Lau CW, Tsang SY, Xu A, Zhu Z, et al. From skeleton to cytoskeleton: osteocalcin transforms vascular fibroblasts to myofibroblasts via angiotensin II and Toll-like receptor 4. *Circ Res*. 2012;111:e55-66.
30. Shi ZD, Ji XY, Qazi H, Tarbell JM. Interstitial flow promotes vascular fibroblast, myofibroblast, and smooth muscle cell motility in 3-D collagen I via upregulation of MMP-1. *Am J Physiol Heart Circ Physiol*. 2009;297:H1225-34.
31. Yeager ME, Frid MG, Stenmark KR. Progenitor cells in pulmonary vascular remodeling. *Pulm Circ*. 2011;1:3-16.
32. Keeley EC, Mehrad B, Strieter RM. Fibrocytes: bringing new insights into mechanisms of inflammation and fibrosis. *Int J Biochem Cell Biol*. 2010;42:535-42.
33. Yue WM, Liu W, Bi YW, He XP, Sun WY, Pang XY, et al. Mesenchymal stem cells differentiate into an endothelial phenotype, reduce neointimal formation, and enhance endothelial function in a rat vein grafting model. *Stem Cells Dev*. 2008;17:785-93.
34. Diez M, Musri MM, Ferrer E, Barbera JA, Peinado VI. Endothelial progenitor cells undergo an endothelial-to-mesenchymal transition-like process mediated by TGFbetaRI. *Cardiovasc Res*. 2010;88:502-11.
35. Tanaka K, Sata M, Hirata Y, Nagai R. Diverse contribution of bone marrow cells to neointimal hyperplasia after mechanical vascular injuries. *Circ Res*. 2003;93: 783-90.